CHALMERS
UNIVERSITY OF TECHNOLOGY

Improving sensitivity through data augmentation with synthetic lymph node metastases for AI-based analysis of PSMA PET-CT images

Downloaded from: https://research.chalmers.se, 2024-10-12 05:42 UTC

Citation for the original published paper (version of record):
Tragardh, E., Ulén, J., Enqvist, O. et al (2024). Improving sensitivity through data augmentation with synthetic lymph node metastases for
AI-based analysis of PSMA PET-CT images. Clinical Physiology and Functional Imaging, 44(4): 332-339. http://dx.doi.org/10.1111/cpf.12879

N.B. When citing this work, cite the original published paper.

research.chalmers.se offers the possibility of retrieving research publications produced at Chalmers University of Technology. It covers all kind of research output: articles, dissertations, conference papers, reports etc. since 2004. research.chalmers.se is administrated and maintained by Chalmers Library

(article starts on next page)

Check for updates

Received: 8 November 2023 | Accepted: 18 March 2024

DOI: 10.1111/cpf.12879

Clinical Physiology and Functional Imaging

ORIGINAL ARTICLE

Improving sensitivity through data augmentation with synthetic lymph node metastases for AI-based analysis of PSMA PET-CT images

Elin Trägårdh[1,2] | Johannes Ulén[3] | Olof Enqvist[3,4] | Lars Edenbrandt[5] | Måns Larsson[3]

[1]Department of Translational Medicine and Wallenberg Centre for Molecular Medicine, Lund University, Malmö, Sweden

[2]Department of Clinical Physiology and Nuclear Medicine, Skåne University Hospital, Malmö, Sweden

[3]Eigenvision AB, Malmö, Sweden

[4]Department of Electrical Engineering, Chalmers University of Technology, Gothenburg, Sweden

[5]Department of Molecular and Clinical Medicine, Institute of Medicine, Sahlgrenska Academy, University of Gothenburg, Gothenburg, Sweden

Correspondence
Elin Trägårdh, Department of Clinical Physiology and Nuclear Medicine, Skåne University Hospital, Carl Bertil Laurells g 9, 205 02 Malmö, Sweden.
Email: Elin.tragardh@med.lu.se

Funding information
Region Skåne; Knut och Alice Wallenbergs Stiftelse; Swedish Cancer Foundation; Allmänna Sjukhusets i Malmö Stiftelse för Bekämpande av Cancer; Swedish Prostate Cancer Foundation

Abstract

Background: We developed a fully automated artificial intelligence (AI)AI-based-based method for detecting suspected lymph node metastases in prostate-specific membrane antigen (PSMA)(PSMA) positron emission tomography-computed tomography (PET-CT)(PET-CT) images of prostate cancer patients by using data augmentation that adds synthetic lymph node metastases to the images to expand the training set.

Methods: Synthetic data were derived from original training images to which new synthetic lymph node metastases were added. Thus, the original training set from a previous study ($n = 420$) was expanded by one synthetic image for every original image ($n = 840$), which was used to train an AI model. The performance of the AI model was compared to that of nuclear medicine physicians and a previously developed AI model. The human readers were alternately used as a reference and compared to either another reading or AI model.

Results: The new AI model had an average sensitivity of 84% for detecting lymph node metastases compared with 78% for human readings. Our previously developed AI method without synthetic data had an average sensitivity of 79%. The number of false positive lesions were slightly higher for the new AI model (average 3.3 instances per patient) compared to human readings and the previous AI model (average 2.8 instances per patient), while the number of false negative lesions was lower.

Conclusions: Creating synthetic lymph node metastases, as a form of data augmentation, on [18F]PSMA-1007F]PSMA-1007 PETPET-CT-CT images improved the sensitivity of an AI model for detecting suspected lymph node metastases. However, the number of false positive lesions increased somewhat.

KEYWORDS

artificial intelligence, machine learning, PET-CT, prostate cancer, PSMA, synthetic data

This is an open access article under the terms of the Creative Commons Attribution-NonCommercial License, which permits use, distribution and reproduction in any medium, provided the original work is properly cited and is not used for commercial purposes.
© 2024 The Authors. *Clinical Physiology and Functional Imaging* published by John Wiley & Sons Ltd on behalf of Scandinavian Society of Clinical Physiology and Nuclear Medicine.

1 | INTRODUCTION

Prostate-specific membrane antigen-ligand (PSMA) positron emission tomography with computed tomography (PET-CT) is an emerging and important method for the correct staging of patients with high-risk prostate cancer, identifying sites of recurrence and determining eligibility for [^{177}Lu]Lu-PSMA treatment. Different diagnostic PSMA radiopharmaceuticals are available, such as [^{68}Ga]Ga-PSMA-11 and [^{18}F]PSMA-1007 (Anttinen et al., 2021; Derwael et al., 2020; Herlemann et al., 2016; Hofman et al., 2020; Hope et al., 2019; Maurer et al., 2016; Perera et al., 2020; Petersen & Zacho, 2020; Seifert et al., 2021). The interpretation relies on visual analysis, so it is subject to inter- and intra-observer variability (Fanti et al., 2017). Artificial intelligence (AI) can help with the standardization of image interpretation, act as a second opinion to nuclear medicine physicians, possibly quantify the PSMA-positive tumour burden before [^{177}Lu]Lu-PSMA treatment, and evaluate the treatment response in consecutive PSMA PET-CT scans (Lindgren Belal et al., 2024).

We have previously developed a fully automated AI-based method for the detection and quantification of suspected prostate tumours and their recurrence, lymph node metastases, and bone metastases in [^{18}F]PSMA-1007 PET-CT scans (Tragardh et al., 2022). Since the training of the AI model relies on manual segmentations of tumour and metastases, increasing the size of the training set is time-consuming. However, a large and varied training set is important for creating good AI. We hypothesized that creating synthetic lymph node metastases as a form of data augmentation, could help with increasing the training data for the AI method without the need for laborious manual segmentations, thus providing the potential to increase the performance of the AI model.

Data augmentation is a common technique used to reduce overfitting; the idea is to slightly modify the input data in a realistic way to improve the generalization of the model. For medical images commonly used augmentation methods are random rotations, scaling, deformations and intensity shifts. To the best of our knowledge, no one has used synthetic data to train AI models for PSMA PET-CT images before. Bergen et al. has previously used generative adversarial networks (GANs) to synthesize head-and-neck [^{18}F]fluorodeoxyglucose PET images (Bergen et al., 2022). They were able to train a network to segment tumours and metastases with only synthesized data but achieved slightly worse results than a network trained on real data.

The aim of this study was to develop a fully automated AI-based method for detecting suspected lymph node metastases in [^{18}F]PSMA-1007 PET-CT in patients with prostate cancer by adding synthetic lymph node metastases to the images to expand the training set. The performance of this method was then compared to that of nuclear medicine physicians and a previously developed AI method (Tragardh et al., 2022) that did not include synthetic data.

2 | METHODS

2.1 | Patients and imaging

The patients and imaging were the same as those in a previous study (Tragardh et al., 2022). In short, the study included 660 patients who were referred for [^{18}F]PSMA-1007 PET-CT at Skåne University Hospital, during 2019–2020. The patients were administered 4 MBq/kg of [^{18}F]PSMA-1007, and images were obtained on a Discovery MI PET-CT system (GE Healthcare) after a 2 h accumulation time. The images were obtained using time-of-flight, point spread function modelling and a 256 × 256 matrix (with a pixel size of 2.7 × 2.7 mm^2 and slice thickness of 2.8 mm).

Images were reconstructed using Q.Clear (GE Healthcare) and a beta factor of 800 (Tragardh, Minarik, et al., 2020). Diagnostic CT with oral and intravenous contrast was performed and used for attenuation correction and anatomic correlation. Images for attenuation correction were acquired in the late venous phase. An adaptive statistical iterative reconstruction algorithm was used. The study was approved by the Regional Ethical Review Board (#2016/417, #2018/117 and #2018/753) and the Swedish Ethical Review Authority (#2021-05734-02). The patients provided written informed consent, and the study followed the principles of the Declaration of Helsinki.

2.2 | Manual segmentations for training

One experienced nuclear medicine physician and radiologist segmented suspected lymph node metastases in the PET-CT images, as described previously (Tragardh et al., 2022). From the full set, 120 studies were used as a test set. Additional data set statistics are shown in Table 1.

2.3 | Synthetic data creation

The synthetic data used in this paper were derived from original training images to which new, synthetic, lymph node metastases

TABLE 1 Data set statistics divided into training (without synthetic data), training synthetic, validation and test splits (with the three different manual segmentations for the test set).

Data set	*n*	*n* empty	mean *n* positives
Training	420	294	1.79
Training synthetic	840	308	2.88
Validation	120	83	1.175
Test reading 1	120	78	2.05
Test reading 2	120	70	2.52
Test reading 3	120	70	2.29

Note: Number of patients (*n*), number of patients without lymph node metastasis (*n* empty) and mean number of lymph node metastasis per patient (mean *n* positives) are shown.

1475097x, 0, Downloaded from https://onlinelibrary.wiley.com/doi/10.1111/cpf.12879 by Statens Beredning, Wiley Online Library on [19/04/2024]. See the Terms and Conditions (https://onlinelibrary.wiley.com/terms-and-conditions) on Wiley Online Library for rules of use; OA articles are governed by the applicable Creative Commons License

were added. Two important aspects were considered when adding synthetic lymph node metastases to training images. Firstly, the synthetic lymph node metastases should be positioned realistically. Secondly, the CT and SUV image values should be realistic for the added metastases. To achieve this, an atlas of lymph node metastases was built using the images in the training set and a manually annotated lymph node positioning mask. The atlas was used to add new, synthetic, lymph node metastasis to existing CT and SUV images. In short, the CT and SUV image values for lymph node metastasis available in the training set were copied to new synthetic training images.

2.4 | Lymph node metastasis atlas

The lymph node metastasis atlas consisted of the following:

1. A lymph-node position mask for a reference CT image.
2. Transformations from the reference CT image to all CT images in the training set.
3. Lymph-node metastasis templates.

Each part of the atlas is described in detail below.

2.5 | Lymph node position mask

To enable realistic positioning of the synthetic lymph nodes, areas where lymph nodes naturally appear were manually annotated in a lymph-node position mask. The annotations were manually done in a reference CT image by an experienced radiologist, as shown in Figure 1. This was the only manual labour needed to create the synthetic data set.

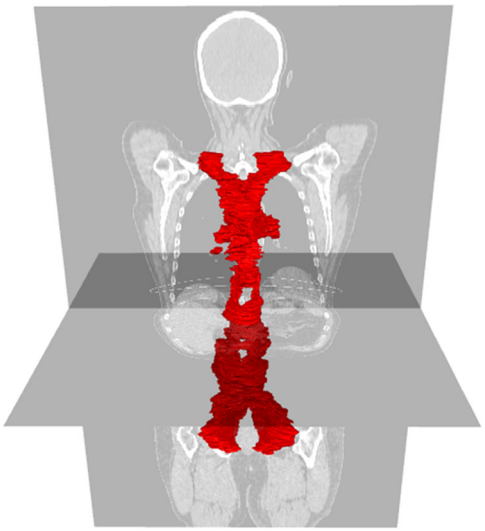

FIGURE 1 Visualization of the manually annotated lymph-node position mask.

2.6 | Spatial transformations

Spatial transformations were calculated between all training images and the reference CT image. Thus, the lymph-node position mask could be transformed from the reference CT to any training image. The spatial transformations were specifically designed with lymph-node positioning in mind. The idea was that the relative position between a lymph node and the surrounding organs should be accurate for the position to appear realistic. To calculate the transformation between a training image and the reference, organs were segmented in both images using only the CT image and the method described in a previous study (Tragardh, Borrelli, et al., 2020). A subset of all segmented organs was then used to align the training image to the CT image by calculating a set of affine transforms using Elastix (Klein et al., 2010). The organs used were the aorta, left lung, right lung, heart, sternum, left hip bone, right hip bone, left femur, right femur and all vertebrae. These organs were chosen as they were located close to the lymph nodes where metastases generally appear and because they can be reliably segmented with high accuracy.

For each organ, an affine transformation that aligns the two images locally was calculated. The surface pixels for all organs in the two images were then matched by first transforming the pixel position of the surface pixels in the reference image using the calculated affine transformation, followed by finding the closest surface pixel in the training image. In addition to the matched points, the local affine transformation without the translation was stored to account for scaling and rotation differences between the two images. The transformations from the four closest organs were used to transfer points between reference and training images. This is described in more detail in a later section.

2.7 | Lymph node metastasis templates

The lymph node templates were extracted from all images in the training set. For each lymph node metastasis in the training set, CT and SUV images as well as annotation patches, were stored as a template. The size of the patch depended on the size of the metastasis annotation and was extended by 15 mm in all directions from the annotation edges. Some lymph node metastases in the training set were excluded since they would be hard to transfer to a new training image in a realistic way. The exclusion criteria used were a maximum metastasis volume of 15 mL and a limitation of only one metastasis that could be present in a patch.

2.8 | Adding synthetic metastases to an image

A synthetic image was created by adding synthetic lymph node metastases to one of the existing training images. Firstly, the number of synthetic metastases that should be added was chosen randomly between 1 and 4. Then, for each synthetic metastasis, two steps were taken: positioning and image augmentation. Note that for a few cases, no valid positions for synthetic lymph nodes could be found, and hence no synthetic data were added.

1475097x, 0, Downloaded from https://onlinelibrary.wiley.com/doi/10.1111/cpf.12879 by Statens Beredning, Wiley Online Library on [19/04/2024]. See the Terms and Conditions (https://onlinelibrary.wiley.com/terms-and-conditions) on Wiley Online Library for rules of use; OA articles are governed by the applicable Creative Commons License

2.9 | Positioning

A centre position was randomly chosen from the reference lymph node position mask. In addition to being placed within the position masks, the centre point of the metastasis was placed at least 15 mm away from any organ or any other tumour or metastasis (synthetic or real). The centre position was transferred to the training image using the organ surface point correspondences and local affine transformations. For all alignment organs, the distance to the closest surface point from the centre position was calculated. In addition, the estimated corresponding position in the training image was calculated using:

$$p_i^T = s_i^T + A_i\left(s_i^T - s_i^R\right)$$

where the subscript i denotes the organ from which the position estimation came, superscripts T and R denote training and reference images, respectively, s denotes the surface positions, and A is the local affine transformation. The translation part of the local affine transformation has been set to identity. The final transformed centre position in the training image was then calculated by:

$$p^T = w_1 p_1^T + w_2 p_2^T + w_3 p_3^T + w_4 p_4^T$$

where the weights w_i were calculated for all organs as the inverse of the distance to the closest surface pixel for that organ. The weights for the four closest organs were then normalized so that they sum to one and used to calculate the transformed centre position.

2.10 | Image augmentation

Once the centre position in the training image of the synthetic metastasis was calculated, a metastasis template was randomly chosen and copied into the image at that position. Before being copied, the CT, SUV and annotation were perturbed by applying a small random rotation and scaling. To avoid introducing sharp edges in the CT and SUV images, the template CT and SUV were added to the training image using a Gaussian weighting map of 1 at the centre position and 0 at the edges. Hence, at the centre position, the new image was identical to the template but closer to the edges. The new image intensities were weighted averages of the template and the original image. The lymph node annotation was added with the same method, but the annotation was not weighted with a Gaussian weighting map as the CT and SUV images were. Figure 2 shows an example of a training image where a synthetic lymph node metastasis has been added.

2.11 | AI tool

The structure and training of the AI tool trained on the real and synthetic images was the same in almost all aspects as what was presented in a previous study (Tragardh et al., 2022). The model was a 3D UNet (Cicek et al., 2016) that segmented the image into four classes: prostate tumour or recurrence, lymph node metastases, bone metastases or background. In addition to the CT and SUV images, a previous organ mask (Tragardh, Borrelli, et al., 2020) was used as input to the network. The training set of the AI tool consisted of the original training set from another study (Tragardh et al., 2022) and one synthetic image for every image in the original training set. The training of the model followed the same procedure as in the other study (Tragardh et al., 2022), but samplings masks for the synthetic training images were not updated using the pixel losses. The sampling mask updates are a good way to find background areas that are difficult for the model to segment correctly. Since the synthetic images were created from the original training images, the difficult background areas were already present in the original images.

2.12 | Model evaluation and statistical analysis

The performance of the AI-based method was assessed by the same test set as in a previous study (Tragardh et al., 2022) and consisted of

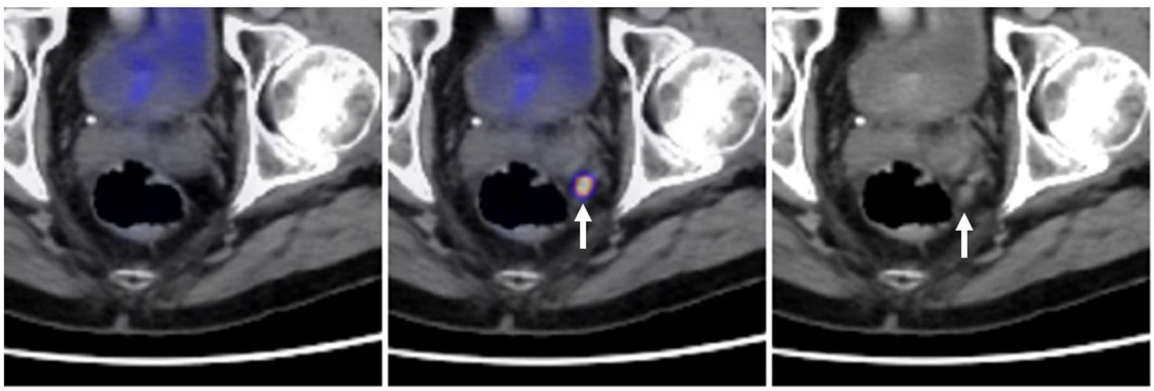

FIGURE 2 Example image of a synthetic lymph node metastasis. Left: The original fused PET-CT image. Centre: Fused PET-CT image with a synthetic lymph node metastasis added on the left side of the pelvis (arrow). Right: CT image with a synthetic lymph node metastasis added (arrow). PET-CT, positron emission tomography-computed tomography.

1475097x, 0, Downloaded from https://onlinelibrary.wiley.com/doi/10.1111/cpf.12879 by Statens Beredning, Wiley Online Library on [19/04/2024]. See the Terms and Conditions (https://onlinelibrary.wiley.com/terms-and-conditions) on Wiley Online Library for rules of use; OA articles are governed by the applicable Creative Commons License

120 patients and three sets of annotations by expert readers. One of the expert readers was the nuclear medicine physician who also performed the segmentations for the model training (denoted as Reading A). Six other nuclear medicine physicians segmented suspected lymph node metastases in 40 cases each from the test set of 120 patients. Thus, each PET-CT in the test set was segmented by two readers who were not involved in the model training (Reading B and Reading C).

The model was evaluated on a lesion-based level to determine the AI model's ability to detect the lymph node metastases identified by one of the three readings. To assess inter-reader variability, the readers were also compared. Readings A, B and C were alternately used as references and compared to either another human reading or to the AI model. True positive lesions for a human reading or the AI model were defined as partial (at least one voxel), or full segmentation (all voxels) overlap with another reading used as the reference; otherwise, they were considered false negative. Lesions detected by a human reading or the AI model without segmentation overlap with the reading used as the reference were regarded as a false positive. The sensitivity was calculated as the proportion of suspected lymph node metastases detected by a human reading or by the AI model out of those detected by the reading used as a reference. The positive predictive value (PPV) was calculated as the proportion of true positive lesions for human readings or by the AI model compared to the reference reading. Specificity and negative predictive value were left out due to the problem of defining meaningful true-negative samples in this kind of study.

3 | RESULTS

The AI model had an average sensitivity of 84% for detecting suspected lymph node metastases, whereas the average sensitivity was 78% for human readings (when each reading was alternately used as a reference). For comparison, our previously developed AI method without synthetic data had an average sensitivity of 79% (Tragardh et al., 2022), as shown in Figure 3. Table 2 shows the number of true positive, false negative and false positive lymph node metastases. The number of false negatives per patient was rather low for both when the AI model and a human reading was compared to a reference reading. For the AI method, the number of true positives was higher, and the number of false negatives lower compared to 'Reading versus Reading.' A higher number of false positive lesions were found when the AI model was compared to human readings compared with 'Reading versus Reading.' When comparing the numbers to our previously published AI method, the new AI method found more true positive lymph node metastases (230 vs. 215) and a lower number of false negative lesions (45 vs. 59) but a higher number of false positive lesions (391 vs. 333).

Of all suspected lymph node metastases segmented by the AI model on the test set, 29.7% were also marked by all three readings. Two of the readings agreed with the AI model in 5.2% of the cases, and one of the readings in 10.1% of the cases. Thus, in 55% of the positive lesions marked by the AI model, none were marked by any of the readings.

Figure 4 shows an example of segmented suspected lymph node metastases for the different readings and AI models.

TABLE 2 True and false positives (TP/FP), false negatives (FN), sensitivity and positive predictive value (PPV) for the detection of lymph node metastases. The numbers show the average and range when one reader at a time was used as a reference.

n = 120 patients	AI synthetic versus reading	AI reference versus reading	Reading versus reading
TP (*n*)			
Total	229.7 (226–233)	215.3 (209–221)	208.7 (198–217)
Per patient	1.9 (1.9–1.9)	1.8 (1.7–1.8)	1.7 (1.7–1.8)
FP (*n*)			
Total	391 (383–397)	333.3 (331–335)	65.7 (32–104)
Per patient	3.3 (3.2–3.3)	2.8 (2.8–2.8)	0.5 (0.3–0.9)
FN (*n*)			
Total	44.7 (20–72)	59.0 (30–93)	65.7 (32–104)
Per patient	0.4 (0.2–0.6)	0.5 (0.3–0.8)	0.5 (0.3–0.9)
Sensitivity (%)	84.3 (76.2–91.9)	79.1 (69.2–87.8)	77.9 (65.6–87.0)
PPV (%)	37.0 (36.3–37.5)	39.2 (38.5–40.0)	78.3 (66.9–87.1)

Abbreviation: AI, artificial intelligence.

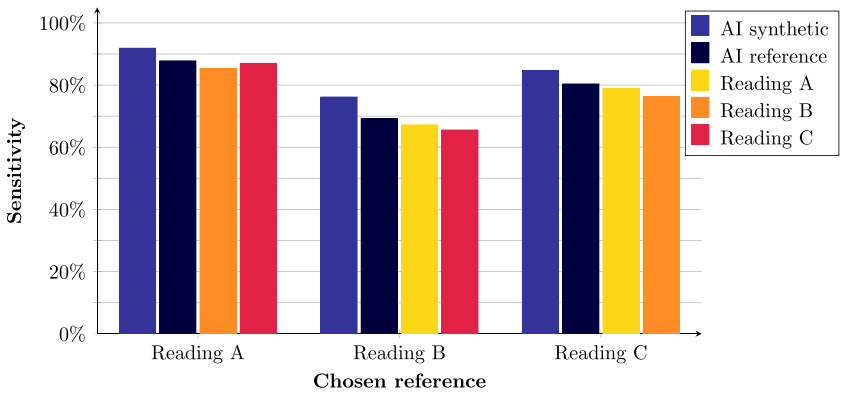

FIGURE 3 Sensitivity for lymph node metastases of the AI model trained with synthetic data, the previously developed AI method, and readings when using Readings A, B and C as a reference. AI, artificial intelligence.

1475097x, 0, Downloaded from https://onlinelibrary.wiley.com/doi/10.1111/cpf.12879 by Statens Beredning, Wiley Online Library on [19/04/2024]. See the Terms and Conditions (https://onlinelibrary.wiley.com/terms-and-conditions) on Wiley Online Library for rules of use; OA articles are governed by the applicable Creative Commons License

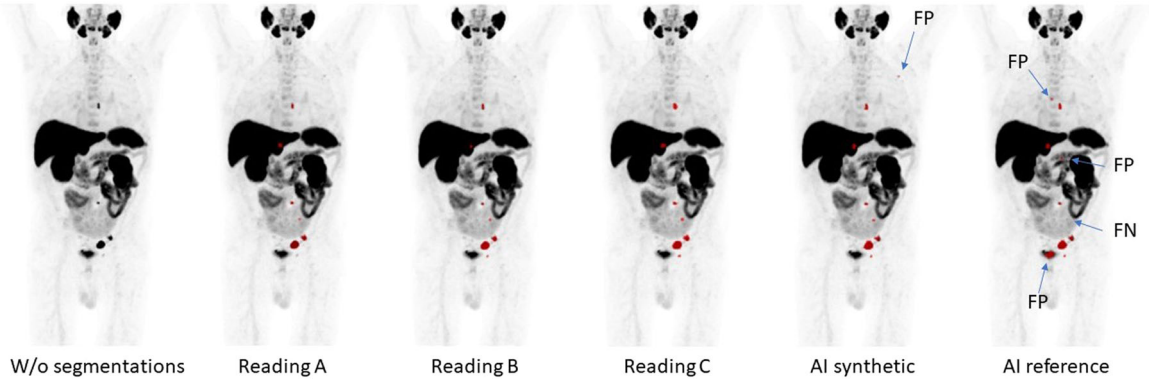

FIGURE 4 A patient example (maximum intensity projections) showing the different segmentations of suspected lymph node metastases in red for the different readings, the AI with synthetic data and the reference AI. False positive (FP) and false negative lesions (FN) for the AI methods are marked. AI, artificial intelligence.

4 | DISCUSSION

In this study, we investigated if data augmentation by adding synthetic lymph node metastases to [^{18}F]PSMA-1007 PET-CT images could improve a fully automated AI method for the detection of suspected lymph node metastases in patients with prostate cancer. By adding synthetic lymph node metastases in our training data, the training set could double in size. The sensitivity and number of true positive lesions were higher compared to a previously published AI method that did not use synthetic data (Tragardh et al., 2022) and compared to nuclear medicine physicians. The number of false negative lesions was lower for the new AI model. However, the false positive lesions increased.

Due to the difficulty of creating large annotated medical data sets, especially for PET-CT images, the approach of synthesizing training data as a form of data augmentation is becoming increasingly popular. However, to the best of our knowledge, no one has used synthetic data in PSMA PET-CT before. In this work, the approach of doing the spatial transformations, focusing on preserving the relative position to nearby organs as accurately as possible, is new, as far as we know. Others have tried different approaches in the field of synthesizing PET training data. For PET image synthesis, Papadimitroulas et al. (2013) used Monte Carlo simulations to generate PET images that capture the heterogeneous activity distributions of tumours. Berthon et al. (2015) developed another Monte Carlo-based simulation method to generate PET images. The generated images were not used for training machine learning models but instead to evaluate existing PET segmentation methods.

The use of GANs has recently become a popular way to create synthetic training data. Jin et al. (2018) simulated lung nodes in CT images using a GAN. They used the synthetic data to train a lung node segmentation network and improved the segmentation accuracy over the baseline training without synthetic data. Tang et al. (2019) used a similar approach to segment lymph nodes in CT images. For PET images, Bergen et al. (2022) used a GAN to synthesize head-and-neck [^{18}F]fluorodeoxyglucose PET images. They trained a network to segment tumours and metastasis with only synthesized data, which achieved slightly worse results than a network trained on real data.

Comparing the AI methods trained with and without synthetic data, the most notable differences were the higher sensitivity and the slightly larger number of false positives for the one trained with synthetic data. We speculate that this is due to the higher rate of lymph node metastases than normal in the synthetic data. This skew in the training set can transfer to the AI model trained on the data. When keeping all other training parameters fixed, there will be a bias for the model, which will segment more areas as lymph node metastases than a model trained without this skew in the training data set. This most likely explains the higher sensitivity and false positive rate. This could possibly be solved by finding more PET-CT scans without lymph node metastases, thus increasing the number of negative examples. It might also be possible to create synthetic negative examples, although care must be taken to make the tissue where a lymph node has been removed seem realistic. We did not try this approach. Unfortunately, specificity on a lesion level cannot be calculated since it is not possible to define meaningful true-negative lesions. The number of false positive lesions with the AI model trained on synthetic data was on average 3.3 per patient. Although somewhat higher than compared with the AI-model without synthetic data (average 2.8 per patient), this should be compared to the CE-marked and FDA-cleared product aPROMISE, which demonstrate a false positive rate of 19.5 per patient for regional lymph node metastases and 90.8 per patient for all lymph node metastases (Johnsson et al., 2022).

This study has some limitations. Only [^{18}F]PSMA-1007 PET-CT images with 2 h accumulation time from a single hospital were used, which probably limits the generalizability of the AI to other patient cohorts. Furthermore, the patients were admitted due to either staging of high-risk prostate cancer or recurrence, so the tumour burden was often low. Thus, the AI might perform worse for patients with a higher tumour burden, such as those with metastatic castration-resistant prostate cancer. Also, no histopathological verification of suspected lymph node metastases exists. In a previous study from our hospital, we assessed the diagnostic accuracy of [^{18}F]PSMA-1007 PET-CT for primary staging of pelvic lymph node metastases before extended lymph node dissection (Ingvar

1475097x, 0, Downloaded from https://onlinelibrary.wiley.com/doi/10.1111/cpf.12879 by Statens Beredning, Wiley Online Library on [19/04/2024]. See the Terms and Conditions (https://onlinelibrary.wiley.com/terms-and-conditions) on Wiley Online Library for rules of use; OA articles are governed by the applicable Creative Commons License

et al., 2022). We found a high specificity of 96% but a low sensitivity (27% for the entire cohort, 54% when only lymph node metastases >3 mm were evaluated). In this study, the AI-tool was trained on the manual segmentations, and it is thus not expected that the AI model performs better than the in-data (human image interpretations).

5 | CONCLUSIONS

It was possible to create synthetic lymph node metastases, as a form of data augmentation, on [^{18}F]PSMA-1007 PET-CT images and thus double the size of the training set for developing a fully automated AI method. The new method had higher sensitivity than experienced nuclear medicine physicians, as well as than a previously developed AI method that did not use synthetic data. However, the PPV was slightly lower due to a higher number of false positive lesions.

ACKNOWLEDGEMENTS

The Knut and Alice Wallenberg Foundation, the Medical Faculty at Lund University, Region Skåne, Malmö General Hospital Foundation, the Swedish Cancer Foundation and the Swedish Prostate Cancer Foundation are acknowledged for their generous financial support. The funders of the study were not involved in the study design, data collection, data interpretation, writing of the report, or the decision to submit the paper for publication. The funders have no commercial interests.

CONFLICT OF INTEREST STATEMENT

J. U., O. E. and M. L. are board members and stockholders of Eigenvision AB, which is a company working with research and development in automated image analysis, computer vision and machine learning. The remaining authors declare no conflict of interest.

DATA AVAILABILITY STATEMENT

The data sets used and/or analysed during the current study are available from the corresponding author upon reasonable request.

ORCID

Elin Trägårdh http://orcid.org/0000-0002-7116-303X
Lars Edenbrandt http://orcid.org/0000-0002-0263-8820

REFERENCES

Anttinen, M., Ettala, O., Malaspina, S., Jambor, I., Sandell, M., Kajander, S. et al. (2021) A prospective comparison of (18)F-prostate-specific membrane antigen-1007 positron emission tomography computed tomography, whole-body 1.5 T magnetic resonance imaging with diffusion-weighted imaging, and single-photon emission computed tomography/computed tomography with traditional imaging in primary distant metastasis staging of prostate cancer (PROSTAGE). *European Urology Oncology*, 4, 635–644.

Bergen, R., Rajotte, J.-F., Yousefirizi, F., Klyuzhin, I., Rahmim, A. & Ng, R. (2022) *3D PET image generation with tumour masks using TGAN*. SPIE.

Berthon, B., Häggström, I., Apte, A., Beattie, B.J., Kirov, A.S., Humm, J.L. et al. (2015) PETSTEP: generation of synthetic PET lesions for fast evaluation of segmentation methods. *Physica Medica*, 31, 969–980.

Cicek, Ö., Abdulkadir, A., Lienkamp, S., Brox, T. & Ronneberger, O. (2016) 3D U-NET: learning dense volumetric segmentation from sparse annotation. In: Ourselin, S., Joskowicz, L., Sabunco, M., Unal, G. & Wells, W. (Eds.) *Medical image computing and computer-assisted intervention-MICCAI 2016*, 9901. Springer.

Derwael, C., Lavergne, O., Lovinfosse, P., Nechifor, V., Salvé, M., Waltregny, D. et al. (2020) Interobserver agreement of [(68)Ga]Ga-PSMA-11 PET/CT images interpretation in men with newly diagnosed prostate cancer. *EJNMMI Research*, 10, 15.

Fanti, S., Minozzi, S., Morigi, J.J., Giesel, F., Ceci, F., Uprimny, C. et al. (2017) Development of standardized image interpretation for 68Ga-PSMA PET/CT to detect prostate cancer recurrent lesions. *European Journal of Nuclear Medicine and Molecular Imaging*, 44, 1622–1635.

Herlemann, A., Wenter, V., Kretschmer, A., Thierfelder, K.M., Bartenstein, P., Faber, C. et al. (2016) (68)Ga-PSMA positron emission tomography/computed tomography provides accurate staging of lymph node regions prior to lymph node dissection in patients with prostate cancer. *European Urology*, 70, 553–557.

Hofman, M.S., Lawrentschuk, N., Francis, R.J., Tang, C., Vela, I., Thomas, P. et al. (2020) Prostate-specific membrane antigen PET-CT in patients with high-risk prostate cancer before curative-intent surgery or radiotherapy (proPSMA): a prospective, randomised, multicentre study. *The Lancet*, 395, 1208–1216.

Hope, T.A., Goodman, J.Z., Allen, I.E., Calais, J., Fendler, W.P. & Carroll, P.R. (2019) Metaanalysis of (68)Ga-PSMA-11 PET accuracy for the detection of prostate cancer validated by histopathology. *Journal of Nuclear Medicine*, 60, 786–793.

Ingvar, J., Hvittfeldt, E., Trägårdh, E., Simoulis, A. & Bjartell, A. (2022) Assessing the accuracy of [18F]PSMA-1007 PET/CT for primary staging of lymph node metastases in intermediate- and high-risk prostate cancer patients. *EJNMMI Research*, 12, 48.

Jin, D., Xu, Z., Tang, Y., Harrison, A.P. & Mollura, D.J. (2018) *CT-realistic lung nodule simulation from 3D conditional generative adversarial networks for robust lung segmentation*. Springer International Publishing, pp. 732–740.

Johnsson, K., Brynolfsson, J., Sahlstedt, H., Nickols, N.G., Rettig, M., Probst, S. et al. (2022) Analytical performance of aPROMISE: automated anatomic contextualization, detection, and quantification of [18F]DCFPyL (PSMA) imaging for standardized reporting. *European Journal of Nuclear Medicine and Molecular Imaging*, 49, 1041–1051.

Klein, S., Staring, M., Murphy, K., Viergever, M.A. & Pluim, J. (2010) elastix: a toolbox for intensity-based medical image registration. *IEEE Transactions on Medical Imaging*, 29, 196–205.

Lindgren Belal, S., Frantz, S., Minarik, D., Enqvist, O., Wikström, E., Edenbrandt, L. et al. (2024) Applications of artificial intelligence in PSMA PET/CT for prostate cancer imaging. *Seminars in Nuclear Medicine*, 54, 141–149.

Maurer, T., Gschwend, J.E., Rauscher, I., Souvatzoglou, M., Haller, B., Weirich, G. et al. (2016) Diagnostic efficacy of (68)Gallium-PSMA positron emission tomography compared to conventional imaging for lymph node staging of 130 consecutive patients with intermediate to high risk prostate cancer. *Journal of Urology*, 195, 1436–1443.

Papadimitroulas, P., Loudos, G., Le Maitre, A., Hatt, M., Tixier, F., Efthimiou, N. et al. (2013) Investigation of realistic PET simulations incorporating tumor patient's specificity using anthropomorphic models: creation of an oncology database. *Medical Physics*, 40, 112506.

Perera, M., Papa, N., Roberts, M., Williams, M., Udovicich, C., Vela, I. et al. (2020) Gallium-68 prostate-specific membrane antigen positron emission tomography in advanced prostate cancer-updated diagnostic utility, sensitivity, specificity, and distribution of prostate-specific membrane antigen-avid lesions: a systematic review and meta-analysis. *European Urology*, 77, 403–417.

Petersen, L.J. & Zacho, H.D. (2020) PSMA PET for primary lymph node staging of intermediate and high-risk prostate cancer: an expedited

1475097x, 0, Downloaded from https://onlinelibrary.wiley.com/doi/10.1111/cpf.12879 by Statens Beredning, Wiley Online Library on [19/04/2024]. See the Terms and Conditions (https://onlinelibrary.wiley.com/terms-and-conditions) on Wiley Online Library for rules of use; OA articles are governed by the applicable Creative Commons License

systematic review. *Cancer Imaging: The Official Publication of the International Cancer Imaging Society*, 20, 10.

Seifert, R., Kessel, K., Schlack, K., Weber, M., Herrmann, K., Spanke, M. et al. (2021) PSMA PET total tumor volume predicts outcome of patients with advanced prostate cancer receiving [(177)Lu]Lu-PSMA-617 radioligand therapy in a bicentric analysis. *European Journal of Nuclear Medicine and Molecular Imaging*, 48, 1200–1210.

Tang, Y.-B., Oh, S., Tang, Y.-X., Xiao, J. & Summers, R. (2019) *CT-realistic data augmentation using generative adversarial network for robust lymph node segmentation*. SPIE

Tragardh, E., Borrelli, P., Kaboteh, R., Gillberg, T., Ulen, J., Enqvist, O. et al. (2020) RECOMIA-a cloud-based platform for artificial intelligence research in nuclear medicine and radiology. *EJNMMI Physics*, 7, 51.

Tragardh, E., Enqvist, O., Ulen, J., Jogi, J., Bitzen, U., Hedeer, F. et al. (2022) Freely available, fully automated AI-based analysis of primary tumour and metastases of prostate cancer in whole-body [(18)F]-PSMA-1007 PET-CT. *Diagnostics (Basel)*, 12, 2101.

Tragardh, E., Minarik, D., Brolin, G., Bitzen, U., Olsson, B. & Oddstig, J. (2020) Optimization of [(18)F]PSMA-1007 PET-CT using regularized reconstruction in patients with prostate cancer. *EJNMMI Physics*, 7, 31.

How to cite this article: Trägårdh, E., Ulén, J., Enqvist, O., Edenbrandt, L. & Larsson, M. (2024) Improving sensitivity through data augmentation with synthetic lymph node metastases for AI-based analysis of PSMA PET-CT images. *Clinical Physiology and Functional Imaging*, 1–8. https://doi.org/10.1111/cpf.12879

1475097x, 0, Downloaded from https://onlinelibrary.wiley.com/doi/10.1111/cpf.12879 by Statens Beredning, Wiley Online Library on [19/04/2024]. See the Terms and Conditions (https://onlinelibrary.wiley.com/terms-and-conditions) on Wiley Online Library for rules of use; OA articles are governed by the applicable Creative Commons License